Conductivity of a medium leads to absorption

Start with Maxwell's equations in matter:

$$\nabla \cdot \vec{D} = 4\pi \rho_f$$
$$\nabla \cdot \vec{B} = 0$$
$$\nabla \times \vec{E} = -\frac{1}{c}\frac{\partial \vec{B}}{\partial t}$$
$$\nabla \times \vec{H} = \frac{4\pi}{c}\vec{J} + \frac{1}{c}\frac{\partial \vec{D}}{\partial t}$$

where $\vec{D} = (1 + 4\pi\chi_e)\vec{E} = \epsilon \vec{E}$

$\rho = \rho_b + \rho_f$

where $\vec{B} = (1 + 4\pi\chi_m)\vec{H} = \mu \vec{H}$

$$\nabla \times (\nabla \times E) = \nabla(\nabla \cdot E) - \nabla^2 E = -\frac{1}{c}\frac{\partial}{\partial t}(\nabla \times B)$$

$$\nabla(\nabla \cdot D) - \nabla^2 D = -\frac{\epsilon\mu}{c}\frac{\partial}{\partial t}(\nabla \times H)$$

Assume no net charge ($\rho_f = 0$). Then $\nabla \cdot D = 0$

$$\nabla^2 D = \frac{\epsilon\mu}{c}\frac{\partial}{\partial t}\left(\frac{4\pi J}{c} + \frac{1}{c}\frac{\partial D}{\partial t}\right)$$

Now conductivity σ is defined as $J = \sigma E$ $\left(J = \frac{\sigma}{\epsilon} D\right)$

$$\nabla^2 D = \frac{\epsilon\mu}{c^2}\frac{\partial^2 D}{\partial t^2} + \frac{4\pi\mu\sigma}{c^2}\frac{\partial D}{\partial t}$$

or $$\nabla^2 E = \frac{\epsilon\mu}{c^2}\frac{\partial^2 E}{\partial t^2} + \frac{4\pi\mu\sigma}{c^2}\frac{\partial E}{\partial t}$$ wave equation with damping term

$$\nabla^2 B = \frac{\epsilon\mu}{c^2}\frac{\partial^2 B}{\partial t^2} + \frac{4\pi\mu\sigma}{c^2}\frac{\partial B}{\partial t}$$ can also be derived

Assume solution of the form $\begin{cases} \vec{E} = \vec{E}_0 e^{i(kx - \omega t)} \\ \vec{B} = \vec{B}_0 e^{i(kx - \omega t)} \end{cases}$ which leads by substitution to:

$$-k^2 = -\frac{\epsilon\mu\omega^2}{c^2} - i\frac{4\pi\mu\sigma\omega}{c^2}$$ (complex wavenumber)

$$\boxed{k = \sqrt{\epsilon\mu}\,\frac{\omega}{c}\sqrt{1 + i\frac{4\pi\sigma}{\omega\epsilon}}}$$

Denote $k = \mathrm{Re}(k) + i\,\mathrm{Im}(k)$

Then $E = E_0 e^{i[\mathrm{Re}(k)x - \omega t]} e^{-\mathrm{Im}(k)x}$

Energy flux $\langle S \rangle = \frac{cE^2}{8\pi} = \frac{cE_0^2}{8\pi} e^{-2\mathrm{Im}(k)x}$ ← attenuation = absorption

"skin depth" $= \frac{1}{2\,\mathrm{Im}(k)}$

In the limit of a poor conductor $\mathrm{Im}(k) << \mathrm{Re}(k)$

$4\pi\sigma << \omega\epsilon$

$k \approx \sqrt{\epsilon\mu}\,\frac{\omega}{c}\left(1 + i\,\frac{2\pi\sigma}{\omega\epsilon}\right)$ poor conductor

A good conductor has $4\pi\sigma >> \omega\epsilon$

$k = \frac{\sqrt{4\pi\sigma\omega\mu}}{c}\sqrt{\frac{\omega\epsilon}{4\pi\sigma} + i}$ Note: If $x << 1$ $\sqrt{x+i} \approx \frac{i+1}{\sqrt{2}}$

$k \approx \frac{\sqrt{2\pi\sigma\omega\mu}}{c}(1+i)$ good conductor

Now the index of refraction is defined as $m = \frac{ck}{\omega}$
So the limiting cases are:

$m \approx \sqrt{\epsilon\mu} + i\,\frac{2\pi\sigma}{\omega}\sqrt{\frac{\mu}{\epsilon}}$ poor conductor

$m \approx \sqrt{\frac{2\pi\mu\sigma}{\omega}}(1+i)$ good conductor

Now extinction is due to both <u>scattering</u> and <u>absorption</u>

$\sigma_e = \sigma_s + \sigma_a$

Define efficiency factors for each process as the ratio of the cross section to the geometrical area of a particle:

$Q_e = Q_s + Q_a$ where $Q_s = \frac{\sigma_s}{\pi r^2}$, $Q_a = \frac{\sigma_a}{\pi r^2}$

ionization of each element will depend on the detailed history, and must be computed at each time before the cooling rate at that time is known. Computations of cooling and recombination have been carried out [18] for a gas heated initially by a distant supernova explosion, assumed to be an intense source of soft (50-eV) X-rays. An alternative transient heating source involves dying stars [19], which are expected to pass through a phase of high ultraviolet luminosity during about 10^6 years, leaving ionized and heated regions behind them after the ultraviolet light source fades away. Such time-dependent effects must certainly be considered in a complete theory for the interstellar gas. However, it is not easy to find a crucial observational test of the complex models which have been computed.

Situations in which a gas is cooling may be unstable against the development of condensations [1, 20], since the cooling function Λ at constant pressure often increases with decreasing T. If a small region becomes colder than its surroundings, it will be compressed to correspondingly higher pressure and will cool more rapidly. However, the condensations formed in this way will be rather small; the requirement of constant pressure limits their size to the sound travel distance during the cooling time, which is at most a few parsecs before compression [20].

REFERENCES

1. G. B. Field, *Ap. J.*, **142**, 531, 1965.
2. L. L. Cowie and C. F. McKee, *Ap. J.*, **211**, 135, 1977.
3. M. J. Seaton, *M.N.R.A.S.*, **119**, 81, 1959.
4. D. E. Osterbrock, *Astrophysics of Gaseous Nebulae*, W. H.Freeman (San Francisco), 1974, Chapt. 3.
5. R. H. Rubin, *Ap. J.*, **153**, 761, 1968.
6. A. Dalgarno and R. A. McCray, *Ann. Rev. Astron. Astroph.*, **10**, 375, 1972.
7. J. P. Ostriker and J. Silk, *Ap. J. (Lett.)*, **184**, L113, 1973.
8. J. Silk, *P.A.S.P.*, **85**, 704, 1973.
9. L. Spitzer and M. G. Tomasko, *Ap. J.*, **152**, 971, 1968.
10. L. Spitzer and E. B. Jenkins, *Ann. Rev. Astron. Astroph.*, **13**, 133, 1975.
11. D. Hollenbach and E. E. Salpeter, *J. Chem. Phys.*, **53**, 79, 1970.
12. T. L. Stephens and A. Dalgarno, *Ap. J.*, **186**, 165, 1973.
13. A. Dalgarno and M. Oppenheimer, *Ap. J.*, **192**, 597, 1974.
14. A. E. Glassgold and W. D. Langer, *Ap. J.*, **193**, 73, 1974.
15. W. D. Watson, *Ap. J.*, **176**, 103, 1972.
16. W. D. Watson, *J. Opt. Soc. Am.*, **63**, 164, 1973.
17. M. Jura, *Ap. J.*, **204**, 12, 1976.
18. H. Gerola, M. Kafatos, and R. McCray, *Ap. J.*, **189**, 55, 1974.
19. J. Lyon, *Ap. J.*, **201**, 168, 1975.
20. J. Schwarz, R. McCray, and R. F. Stein, *Ap. J.*, **175**, 673, 1972.

$10^{-(1.086/2.5)} = e^{-1}$

L. Spitzer "Physical Processes in the Interstellar Medium"

7. Optical Properties of Grains

Dust grains scatter and absorb light in interstellar space. In addition, these small solid particles emit radiation at wavelengths much greater than those of the absorbed light. Knowledge of the optical properties of grains can be used to interpret the observed effects in terms of the nature and spatial distribution of these particles.

We discuss briefly some basic concepts of this subject. First we consider the "extinction," here defined as the sum of absorption and scattering; a collimated beam of light can be extinguished by either process. The rate of extinction is again given by equation (3-1). In the discussion of atomic processes the quantity κ_ν in this equation is generally called an absorption coefficient, even though the photon may be promptly reemitted, producing scattering; here κ_ν is called an "extinction coefficient." In measuring light from a single star one normally observes the flux $\mathcal{F}_\nu$, defined as the integral of I_ν over the solid angle of the stellar image. Since the light scattered or emitted by interstellar grains usually makes a negligible contribution to I_ν within a stellar image, the second term on the right-hand side of equation (3-3) may be ignored. If we express the optical thickness τ_ν, in terms of s_ν, the extinction coefficient per particle, in accordance with equation (3-14), then equation (3-3) yields for A_λ, the interstellar extinction in magnitudes at the wavelength λ,

$$A_\lambda = -2.5 \log \frac{\mathcal{F}_\nu}{\mathcal{F}_\nu(0)} = 1.086 \tau = 1.086 N_d Q_e \sigma_d, \qquad (7\text{-}1)$$

where $\mathcal{F}_\nu(0)$ is the stellar flux at the Earth in the absence of extinction, N_d is the number of dust grains per cm^2 along the line of sight from the Earth to the star, and σ_d is the geometrical cross section of a single grain. We use the subscript d throughout to denote dust grains. The dimensionless

quantity Q_e is the "extinction efficiency factor," defined in terms of the optical cross section s_ν by the relationship

$$Q_e = \frac{s_\nu}{\sigma_d}. \tag{7-2}$$

The extinction efficiency of the grains and the resulting extinction both depend on λ. These equations are based on the assumption that all the grains are identical. In the actual case equation (7-1) must be integrated over all the parameters characterizing the grains, including chemical composition, size, shape, and orientation.

Next we consider scattering of light by grains over an appreciable area of the sky, producing a diffuse source of illumination. In this case it is the intensity I_ν, rather than the flux $\mathcal{F}_\nu$, that is observed, and the emissivity for scattered light, which we denote by $j_{\nu S}$, makes the interesting contribution in equation (3-3). We define a "scattering efficiency factor" Q_s, so that a fraction Q_s/Q_e of the light extinguished is scattered rather than absorbed; this fraction is called the "albedo." We may write

$$j_{\nu S}(\kappa) = n_d Q_s \sigma_d \int I_\nu(\kappa') F(\kappa - \kappa')\, d\omega', \tag{7-3}$$

where κ' and κ are unit vectors indicating the directions of the incident and scattered photons, $d\omega'$ is an interval of solid angle about κ', and $F(\kappa - \kappa')$ is a phase function, which we may assume depends on the angle ϕ between κ and κ'; the integral of F over all $d\omega'$ is unity.

Finally we consider the thermal emission from the grains. If we denote by Q_a the corresponding efficiency factor for pure absorption, evidently equal to $Q_e - Q_s$, then use of Kirchhoff's law, equation (3-5), gives for $j_{\nu E}$, the coefficient for thermal emission

$$j_{\nu E} = n_d Q_a \sigma_d B_\nu(T_s), \tag{7-4}$$

where T_s is the temperature of the solid material in the grain. In accordance with the discussion in Section 2.4, the validity of this equation results from the fact that energy is interchanged among the different modes of vibration of the solid grain much more rapidly than between these modes and the radiation field.

In the first section below, the extensive calculations of the optical efficiency factors Q_e, Q_s, and Q_a for spherical particles are summarized. Subsequent sections discuss the use made of these results in interpreting the observations of extinction, scattering, and thermal emission from interstellar grains.

7.1 OPTICAL EFFICIENCY FACTORS

The Mie theory of scattering and absorption by spheres with a complex index of refraction, m, has been applied numerically to a wide variety of cases [1]. Here we give a few typical results and discuss in particular the asymptotic behavior for spheres whose radius a is much larger or much smaller than the wavelength. It is customary to express the size of the sphere in terms of the dimensionless parameter x defined by

$$x = \frac{2\pi a}{\lambda}. \tag{7-5}$$

In Fig. 7.1 are shown values of Q_e for spheres with four different values for m, the index of refraction: (a) $m = \infty$, corresponding to an infinite dielectric constant; (b) $m = 1.33$, corresponding to ice particles (at visual wavelengths); (c) $m = 1.33 - 0.09i$, corresponding to ice with absorbing impurities, or "dirty ice"; (d) $m = 1.27 - 1.37i$, corresponding to spheres of iron. The horizontal scale is x; as m approaches unity, the curves for Q_e shift to the right by an amount proportional to $1/(m-1)$. For small x, the scattering efficiency factor Q_s becomes very small; if mx is much less than unity, we have the usual formula for Rayleigh scattering

$$Q_s = \frac{8}{3} x^4 \left| \frac{m^2 - 1}{m^2 + 2} \right|^2, \tag{7-6}$$

while Q_a in this case is given by

$$Q_a = -4x\, Im\left(\frac{m^2 - 1}{m^2 + 2} \right), \tag{7-7}$$

where Im indicates that the imaginary part is to be taken. When m is purely real (spheres a and b in Fig. 7.1), Q_a vanishes, but for spheres c and d most of the extinction at low x results from absorption, giving rise to a linear variation of Q_e with x in accordance with equation (7-7). As a result, for the spheres with $m = 1.33$, typical of ice, the introduction of a small imaginary part in m much increases Q_e for small x. It may be noted that for the ice sphere the large-scale oscillation of Q_s with changing x, which is due to interference between the transmitted and diffracted radiation, is much reduced when absorption within the sphere is assumed.

Figure 7.1 shows that as x increases, Q_e approaches an asymptotic value of about 2, both for absorbing and for dielectric spheres, while for absorbing spheres Q_a approaches a value somewhat less than unity as expected. Thus twice as much energy is removed from the beam as is

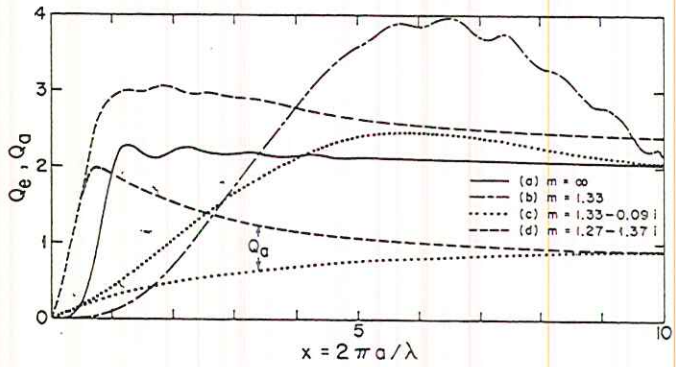

Figure 7.1 Extinction and absorption cross section for spheres. For each value of m, the index of refraction, the upper curves show Q_e, the ratio of extinction and geometrical cross sections, for spheres; x is the ratio of the circumference, $2\pi a$, to the wavelength, λ, of the incident radiation. For cases (c) and (d), with complex values of m, lower curves show Q_a, the corresponding ratio of absorption cross section to πa^2. These theoretical curves [1] are based on exact computations for cases (a), (b), and (d), but for case (c), on an approximate theory, valid for small $m-1$.

actually striking a large sphere. The reason for this behavior is that, in accordance with Babinet's principle, the diffraction pattern due to an obstacle is identical with that of an aperture of the same cross section, and thus contains the same energy as is striking the obstacle. The diffracted energy can be regarded as removed from the incident beam if two requirements are met. First, energy measurements must be made at such great distances behind the obstacle that the shadow has been "washed out," and the Fraunhofer pattern is applicable. Secondly, the diffraction angles must exceed both the initial angular spread of the incident beam and the angular resolution of the detection apparatus.

Evidently this diffracted light accounts for at least half of the energy scattered by a large sphere, with the rays passing through the sphere accounting for the other half if the material is nonabsorbing. We evaluate the contribution of this diffracted radiation to the phase function F, which occurs in equation (7-3) for the scattered light. If a spherical grain is considered, F is a function $F(\phi)$ of the angle ϕ between the incident light and the direction of the scattered or diffracted light; according to equation (7-3), $F(\phi)\,d\omega$ is the fraction of the scattered light energy which at great distances is traveling within a small cone, of solid angle $d\omega$, at an angle ϕ to the direction of the incident beam of light. The diffracted component of this radiation follows closely the Fraunhofer diffraction pattern for a circular aperture with a radius a equal to the radius of the sphere, and we

have the familiar result,

$$F(\phi)=\frac{J_1^2(x\sin\phi)}{\pi\sin^2\phi}. \tag{7-8}$$

The normalization is exact only in the limit as x becomes large. In this equation $J_1(u)$ denotes a Bessel function of order 1, which approaches $u/2$ as u falls below unity. If we denote by ϕ_1 the value of ϕ at which $F(\phi)$ falls to half its central value, we obtain, if ϕ_1 is sufficiently small so that $\sin\phi_1$ may be replaced by ϕ_1,

1st minimum occurs at $x\sin\phi = 1.22\pi$ or $\phi = 0.61\lambda/a$

$$\phi_1=\frac{1.617}{x}=0.257\frac{\lambda}{a}. \tag{7-9}$$

The total scattered light includes radiation which has been refracted through the sphere, and which is not included in equation (7-8). However exact computations [1] for a sphere with m equal to 1.33 show that equation (7-9) gives ϕ_1 rather accurately for the total scattered light when x is between 2 and 5.

The integral of Q_e over all λ can be obtained from the Kramers-Kronig relationship [2, 3], which for a spherical grain gives

$$\int_0^\infty Q_e\,d\lambda=4\pi^2 a\left\{\frac{\varepsilon_0-1}{\varepsilon_0+2}\right\}\equiv 4\pi^2 a F_K, \tag{7-10}$$

where ε_0, the dielectric constant of the grain in the low-frequency limit, equals the square of m, the index of refraction; F_K is defined by equation (7-10). For spheroidal particles F_K is increased [3], but even for a two-to-one ratio of axes and ε_0 as great as 4, the increase is less than about 5 percent. If equation (7-1) is used to eliminate Q_e, and we let $\rho_s 4\pi a^3 N_d/3 = \rho_d L$, where ρ_s is the density of solid material within the grain, and ρ_d is the mean density of dust along the line of sight, of length L, equation (7-10) becomes

$$\rho_d=\frac{1.01\times10^{-23}\rho_s}{F_K}\int_0^\infty\frac{A_\lambda\,d\lambda(\text{cm})}{L(\text{kpc})}. \tag{7-11}$$

The optical properties of nonspherical grains have also been considered [2, 4]. If the grains are aligned, the extinction differs for the two degrees of polarization (see Chapter 8) and in addition the extinction coefficients vary with the direction of the incident radiation. In the absence of alignment, the presence of grains with complex shapes apparently has no very large effect on the mean optical efficiency factors [4].

obtained [16] with a three-component model, taking into account the variation with λ of the index of refraction m of each component. Small graphite grains ($\bar{a}=2.5\times10^{-6}$ cm) have been included to fit the observed peak in the extinction curve at this wavelength. Grains of SiC ($\bar{a}=7.5\times10^{-6}$ cm) have been added to fit the visual and infrared regions, whereas smaller magnesium and aluminum silicate grains ($\bar{a}=4.5\times10^{-6}$ cm) yield

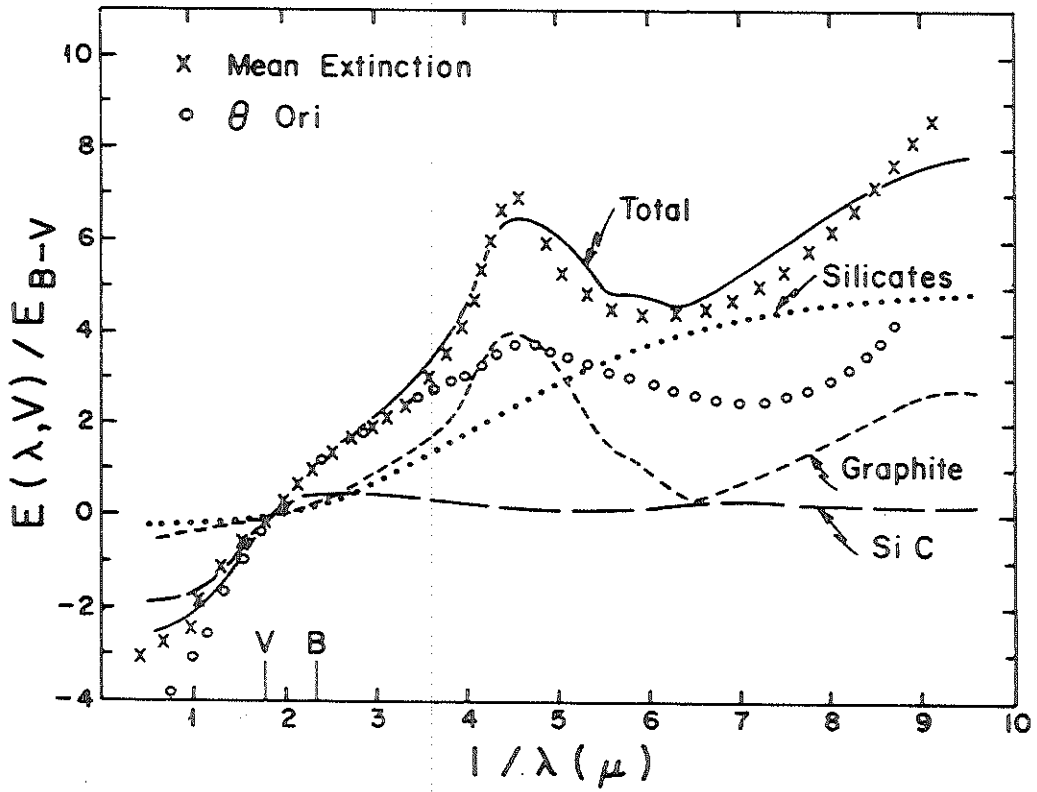

Figure 7.2 Dependence of selective extinction on wavelength. The ratio of $E(\lambda, V)$ to E_{B-V} is plotted against the reciprocal wavelength in microns. The crosses give the mean observed extinction for normal stars [2]; in the ultraviolet these are based on 14 observed stars, excluding 3 abnormal ones; the circles give observed values for $\theta^1+\theta^2$ Ori, showing abnormal extinction. The other curves are computed theoretically [16] for grains of three different types (see text), with the sum of the three shown by the solid line.

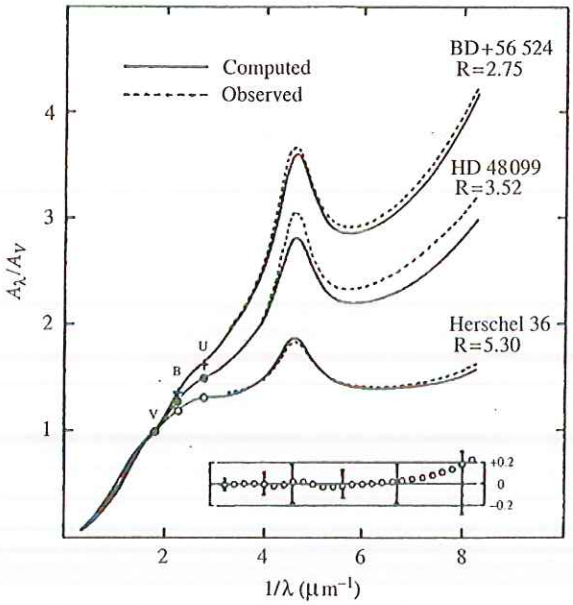

Figure 5.7 Three observed extinction curves are shown as a function of λ^{-1}. These curves show the range in wavelength behavior of the extinction laws in the interstellar medium. The solid lines show, for comparison, the computed parameterized extinction. The insert shows the deviations. Figure courtesy of J. S. Mathis; reprinted with permission from *Ann. Rev. Astron. Astrophys.*, **28**, p. 37, ©1990 by *Ann. Rev.* (www.annualreviews.org).

in the range 4–6. Figure 5.7 compares observed extinction curves in different environments with the R_V-parameterized curve.

Structure in the extinction curve can provide important clues to the nature of the absorbing materials. The ultraviolet bump is the most prominent feature of the interstellar extinction curve. Its peak position is very constant ($\lambda_p = 2175$ Å with a mean deviation of 9 Å). The width of the bump varies much more widely with a typical value of 480 Å but extremes of 360 and 770 Å. After subtraction of an underlying linear continuum extinction, the 2175 Å feature is well represented by a so-called Drude profile, characteristic for absorption associated with a resonance in a conductor.

The visible extinction curve shows weak fine structures, called the diffuse interstellar bands (DIBs), with typical widths of 1–20 Å and strengths $< 0.01\ A_V$. Some 200 bands have been discovered, spanning the wavelength range of the near-UV (4300 Å) to the far-red (~1 μm). These bands are now generally thought to be due to absorption by large molecules rather than dust (cf. Section 6.7.4).

Several absorption features are present in the infrared (cf. Fig. 5.8). The 9.7 μm feature is the strongest one – $\tau_{9.7}/A_V = 18.5$ in the solar neighborhood. This band

A. G. G. M. Tielens
"The Physics and Chemistry of the Interstellar Medium"

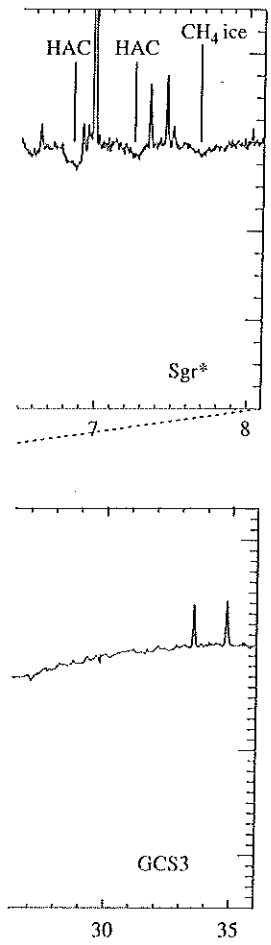

ow strong absorption
e shown here on an
me of these features
rbon [HAC] bands),
H_2O, NH_3, and CH_4
dia. Figure courtesy
7, p. 749.

mpanied by a slightly
ature at about 18 μm.
acteristic substructure.
of absorption features
ving on the dust grains
are discussed in detail

5.3.2 *Scattered light*

As reflection nebulae attest, interstellar dust grains are efficient scatterers of radiation. Adopting a geometry for the nebula and star, the scattering properties of the dust can be derived. Because of the uncertainties in geometry, derived properties are limited to the scattering cross section, or the albedo, and the mean value of the cosine of the scattering angle. The albedo is shown in Fig. 5.9. The albedo is quite high, $\simeq$0.6, and relatively constant in the visible region of the spectrum. Thus, because the extinction rises throughout the visible, the scattering cross section has to increase rapidly towards shorter wavelengths as well. This gives reflection nebulae their characteristic blue color. The broad dip in the albedo curve occurs at the position of the 2175 Å bump in the extinction curve and demonstrates that this is an absorption feature. Likewise, the rapid drop in the albedo at the shortest wavelengths implies that the far-UV rise is an absorption phenomenon. The mean value of the cosine of the scattering angle is about 0.6 in

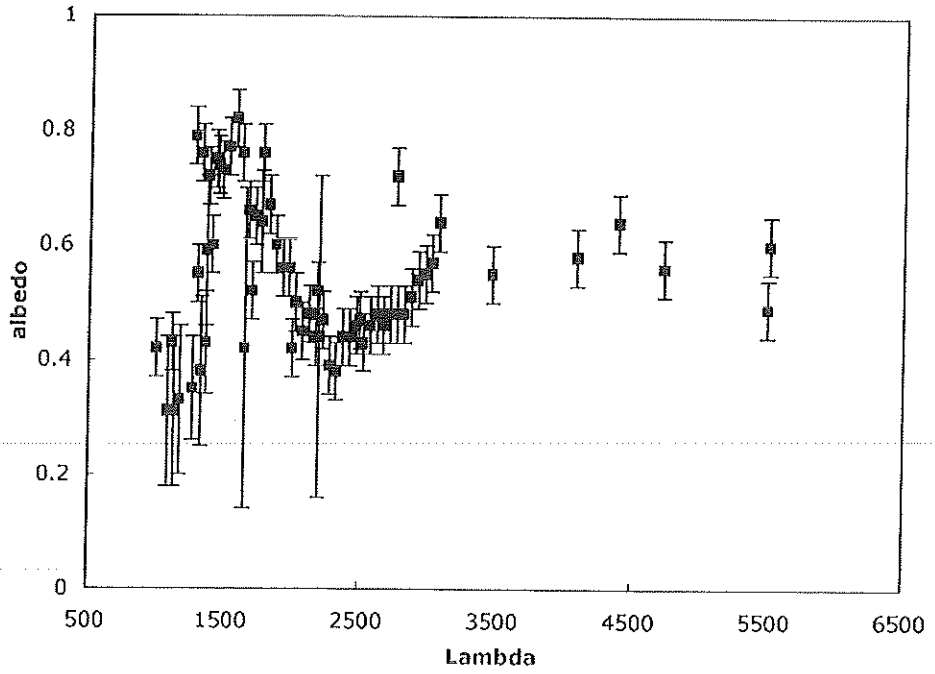

Figure 5.9 The measured albedo of interstellar dust. Note the fairly constant albedo throughout the visible, the presence of the "dip" at the location of the 2175 Å extinction feature, and the rapid drop towards shorter wavelengths. Figure adapted from K. Gordon, 2004, in *Astrophysics of Dust*, ASP Conference Series Vol **309**, ed. Adolf N. Witt, Geoffrey C. Clayton, and Bruce T. Draine, (San Francisco: Astronomical Society of the Pacific), pp. 77–91.

the visible (i.e., strong forward scattering) and decreases to shorter wavelengths (i.e., more isotropic scattering).

5.3.3 *Interstellar polarization*

Linear polarization

Polarization of starlight is due to propagation of light in a medium where the grains are elongated (the cross section is larger in one direction than in the other) and (partially) aligned. Linear polarization curves rise slowly with decreasing wavelength until they reach a maximum, typically in the visible, and then fall more rapidly (cf. Fig. 5.10). Clearly, the polarization behavior is quite different from the extinction behavior of interstellar dust. Empirically, the linear polarization curve in the visible through near-UV range is given by the so-called Serkowski law,

$$p(\lambda) = p(\lambda_{max}) \exp[-K \ln^2(\lambda/\lambda_{max})], \tag{5.92}$$

where λ_{max} is the wavelength of the maximum polarization and K is given by

$$K = 1.86\lambda_{max} - 0.1. \tag{5.93}$$

The wavelength of maximum polarization, λ_{max}, is in the range 0.34 to 1μm with an average of 0.55 μm. It is reasonably well correlated with the total-to-selective extinction ratio, R_V,

$$\lambda_{max}(\mu m) = (0.17 \pm 0.05) R_V. \tag{5.94}$$

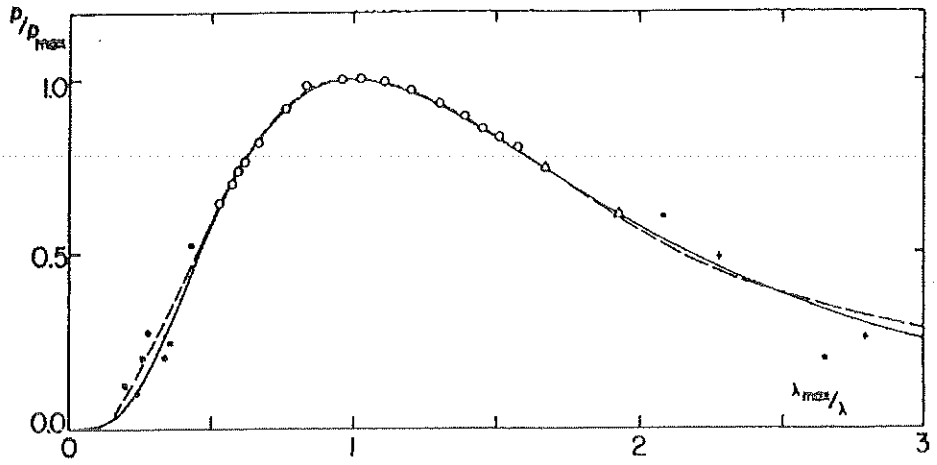

Figure 5.10 The normalized interstellar polarization curve as a function of the normalized wavelength (actually frequency) with $p(\lambda_{max})$ the maximum polarization at the wavelength, λ_{max}.

23. J. A. Hackwell and R. D. Gehrz, *Ap. J.*, **194**, 49, 1974.
24. A. Sandage, *Publ. Astr. Soc. Pacific*, **87**, 853, 1975.
25. E. P. Ney, D. W. Strecker, and R. D. Gehrz, *Ap. J.*, **180**, 809, 1973.
26. L. J. Caroff, V. Petrosian, E. E. Salpeter, R. V. Wagoner, and M. W. Werner, *M.N.R.A.S.*, **164**, 295, 1973.
27. B. T. Lynds, *Ap. J. Supp.*, 7, 1, 1962.
28. B. J. Bok, C. S. Cordwell and R. H. Cromwell, *Dark Nebulae, Globules and Protostars*, B. T. Lynds, Editor, University of Arizona Press, 1971, p. 33.
29. P. Thaddeus, *Star Formation*, IAU Symp. No. 75, T. de Jong and A. Maeder, Editors, D. Reidel Publ. Co. (Dordrecht, Holland), 1977, p. 75.
30. B. Zuckerman and P. Palmer, *Ann. Rev. Astron. Astroph.*, **12**, 279, 1974.
31. R. L. Dickman, *Ap. J.*, **202**, 50, 1975.
32. C. F. Lillie and A. N. Witt, *Ap. J.*, **208**, 64, 1976.
33. D. E. Osterbrock, *Astrophysics of Gaseous Nebulae*, W. H. Freeman (San Francisco), 1974, Section 7.3.
34. C. Sarazin, *Ap. J.*, **220**, 1978, in press.
35. T. de Jong, F. P. Israel, and A. G. G. M. Trilens, *Lecture Notes in Phys.*, J. Springer (Berlin), **42**, 1975, p. 123.
36. N. Panagia, *Astron. Astroph.*, **42**, 139, 1975.
37. E. L. Wright, *Ap. J.*, **185**, 569, 1973.
38. N. Panagia, *Ap. J.*, **192**, 221, 1974.

L. Spitzer "Physical Properties in the Interstellar Medium"

8. Polarization and Grain Alignment

Measurement of the linear polarization of starlight requires a determination of the intensity I_μ in some wavelength band as a function of the direction μ of the electric vector in the radiation. If I_μ varies from a maximum value I_{max} to a minimum value I_{min} as the direction of the electric vector passed by the polarimeter is rotated about the direction κ of propagation, the polarization P is defined by

$$P = \frac{I_{max} - I_{min}}{I}, \tag{8-1}$$

where the total intensity I of the beam is given by

$$I = I_{max} + I_{min}. \tag{8-2}$$

Frequently $100P$, the percentage polarization, is used. Alternatively, the polarization may be expressed in magnitudes and denoted by p; if P is small, $p = 2.17P$. The circular polarization, denoted by V/I, is also defined by an equation similar to (8-1), but with I_r and I_l, the intensity for right-handed and left-handed circular polarization, replacing I_{max} and I_{min}. Sometimes the polarized light is characterized by the four Stokes parameters, I, V, Q, and U, where these last two quantities are defined in equations (8-7) and (8-8).

Plane polarization has been observed in many distant stars [1], with values of P ranging up to a maximum of about 0.07. The direction of the electric vector for which I_μ equals I_{max} tends to be parallel to the galactic plane. The plane defined by this direction of the electric vector and the

direction of propagation κ is called the "plane of vibration." The circular polarization V/I produced by interstellar grains is much weaker, about 10^{-4}, and has been observed in only a few stars.

Here we discuss first the optical properties of elongated grains, since it is presumably such nonspherical particles that are responsible for the polarization. Subsequent sections treat the observed polarization and the possible methods which have been proposed for aligning the grains.

8.1 OPTICAL PROPERTIES OF NONSPHERICAL PARTICLES

For a nonspherical particle, the efficiency factors defined in Section 7.1 will depend on the orientation of the particle with respect both to κ and the direction of the electric vector **E**. Because of the enormous variety of possible shapes for interstellar grains, and because of computational complexities, such efficiency factors have been determined mostly for infinite cylinders [2, 3] (with all cross sections taken per unit length) and for spheroids [3, 4], both of which are axially symmetrical. We denote by Q_{eE} or Q_{eH} the values of Q_e when the plane defined by κ and the axis of symmetry contain the electric or the magnetic vector, respectively, of the radiation. Values of these two efficiency factors for infinite cylinders are shown [3] in Fig. 8.1 for m equal to 1.33 in the simple case where the wave front is parallel to the cylinder axis; Q_{eE} and Q_{eH} now refer to waves for which the electric vector is parallel and perpendicular, respectively, to the cylinder axis. Figure 8.1 shows that Q_{eE} tends to exceed Q_{eH} for wavelengths appreciably longer than the cylinder radius ($x<2\pi$); under these conditions radiation is more strongly scattered when **E** is parallel to the cylinder axis, permitting currents in the grain to flow without building up an opposing electrostatic field. For $x<1$, perfectly reflecting cylinders ($m=\infty$) behave as small antennae, and Q_{eE}/Q_{eH} approaches infinity as x goes to zero. For dielectric cylinders, the addition of some absorption (a small imaginary component of m) changes Q_{eE} and Q_{eH} in much the same way as Q_e is changed for a sphere [compare curves (b) and (c) in Fig. 7.1]; however, $Q_{eE}-Q_{eH}$ is not much altered.

As $(m-1)$ increases, the curves of Q_{eE} and Q_{eH} shift to smaller x, exactly as in Fig. 7.1. Thus for an infinite cylinder with $m=2^{1/2}(1-i)$, Q_{eE} and Q_{eH} are close to their maximum value of about 2 for $x\geqslant 1$, whereas $10(Q_{eE}-Q_{eH})$ reaches its maximum value of about 7 at $x\approx 0.3$ [2].

For spheroids the optical properties have been measured in the laboratory at microwave frequencies with model spheroids scaled to give the correct $2\pi a/\lambda$, where a is the semiminor axis. For a prolate spheroid with its axis of symmetry perpendicular to κ and with its semimajor axis b equal

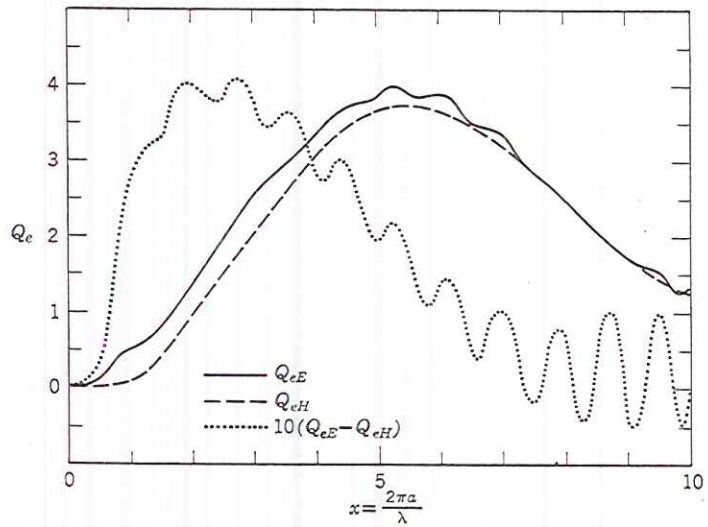

Figure 8.1 Extinction cross sections for cylinders. The theoretical curves [3] show Q_{eE} and Q_{eH}, the extinction efficiency factors for cylinders whose axes are parallel to the electric or magnetic vectors, **E** or **H**, respectively, in the incident radiation. The direction of propagation is taken to be perpendicular to the cylinder axis; a is the cylinder radius, and m, the index of refraction within the cylinder, is assumed to be 1.33.

to $2a$, the measured values [3] of Q_{eE} and Q_{eH} are not very different from the theoretical values for an infinite cylinder of the same index of refraction, with a radius equal to a. In particular, the values of $Q_{eE}-Q_{eH}$ for such spheroids are generally at least half or more of the corresponding values for the cylinders. Comparable results have also been obtained from the exact theory [4], based on solutions of the wave equation in spheroidal coordinates.

The polarizing effectiveness of cylindrical particles with m, the index of refraction, equal to 1.33 is summarized [3] in Table 8.1. We define the quantity r_p as the ratio of $Q_{eE}-Q_{eH}$ to $\overline{Q}_e$, where $\overline{Q}_e$ is defined as $(Q_{eE}+Q_{eH})/2$. As may be seen from equation (8-5) below, $0.46r_p$ is the

Table 8.1. Polarizing Effectiveness of Infinite Cylinder

x	1	2	3	4	5
$\overline{Q}_e$ $(m=1.33)$	0.285	1.11	2.20	3.18	3.76
$0.46r_p$	0.48	0.17	0.078	0.039	0.023

ratio of polarization to extinction in the ideal case where cylindrical grains are all aligned with their axes parallel to each other and perpendicular to the line of sight. For metallic absorbing cylinders with $m=2^{1/2}(1-i)$, the range of values of r_p is roughly similar, but the corresponding values of x are about one-fifth as great.

8.2 OBSERVED POLARIZATION

Extensive measures of P have been made for many stars at a few wavelengths [1] and over most of the accessible spectrum for a few stars [5]. The relationship between P and the observed extinction and the variation of P with wavelength λ can be interpreted in terms of the intrinsic properties of the particles and the extent of their alignment. The variation over the sky both of P and of the direction of polarization gives information on the magnetic field. We discuss here each of these aspects of the observations, with a brief treatment of circular polarization at the end of this section.

a. Dependence on Color Excess

In general, unreddened stars show no polarization to within the observational error. For stars with a large color excess, the values of P show a wide distribution, ranging somewhat uniformly from zero up to a maximum value [1, 3] given by

$$\left(\frac{P}{E_{B-V}}\right)_{\max}=0.090\ \text{mag}^{-1}; \tag{8-3}$$

here P is measured at visual wavelengths, where the dependence on wavelength is generally very small [S8.2b]. The mean value of P/E_{B-V} for observed O and B stars is about half this upper limit.

This correlation between P and E_{B-V} provides strong evidence that extinction by grains is responsible for the observed polarization, and we proceed to express P in terms of the grain properties. If we denote by $Q_{e\max}$ and $Q_{e\min}$ the maximum and minimum mean values of Q_e as the electric vector is rotated, combination of equations (8-1) and (3-3), with $j_\nu=0$, followed by use of equations (3-2), (7-2), and (3-14), gives

$$P=\tfrac{1}{2}N_d\sigma_d(Q_{e\,\max}-Q_{e\,\min}), \tag{8-4}$$

provided that $P\ll 1$ so that only the linear term in $(Q_{e\,\max}-Q_{e\,\min})$ need be retained in expanding the exponent. If we use equation (7-1) to eliminate

$N_d\sigma_d$, we find the relation

$$\frac{P}{A_\lambda}=0.46\frac{(Q_{e\,\max}-Q_{e\,\min})}{\bar{Q}_e}, \tag{8-5}$$

where $\bar{Q}_e$ is again the mean of $Q_{e\,\max}$ and $Q_{e\,\min}$.

If the grains are identical cylinders or highly elongated spheroids, aligned exactly parallel to each other, and perpendicular to the line of sight, $Q_{e\,\max}$ and $Q_{e\,\min}$ will equal Q_{eE} and Q_{eH}, respectively, and P/A_λ will equal $0.46r_p$, whose values are given in Table 8.1 above. If we set A_V/E_{B-V} equal to 3, then equation (8-3) for the peak observed polarization gives $(P/A_V)_{\max}=0.030$. Comparison between the observed and theoretical wavelength dependence of polarization shows [S8.2b] that $x=2.5$ at 5500 Å if the grains are taken to be cylinders with $m=1.33$; for this value of x, Table 7.1 gives $0.46r_p=0.12$, about four times the observed peak value, and eight times the average value of 0.015 for P/A_V. If a greater m is assumed, x is reduced, but the resultant polarizing effectiveness at the V wavelength is not greatly changed. In fact, not all grains will be sufficiently elongated to produce so much polarization nor will the alignment be perfect. These two effects, perhaps with others also, reduce the actual peak value of P/A_V well below its ideal theoretical value.

b. Dependence on Wavelength

Over the wavelength range from 4000 to 6000 Å, the linear polarization, which we denote by $P(\lambda)$, is remarkably flat for most stars, but falls off at shorter or longer wavelengths. Extensive measures of $P(\lambda)$ over a wide spectral range for many stars indicate that the wavelength of maximum polarization, denoted by $\lambda_{\max}$, differs for different stars, with observed values ranging mostly between 4500 and 8000 Å [5], averaging about 5500 Å. However, if the polarization is expressed as a function of $\lambda/\lambda_{\max}$, and divided by $P(\lambda_{\max})$, then the normalized polarization curves for all stars are identical.

The normalized points obtained in this way are plotted in Fig. 8.2 [5]. The open circles in the middle of the spectral range represent averages over groups of 10 to 20 stars, whereas the solid circles represent data for single stars. The curve represents a theoretical calculation of $P(\lambda)$ for partially aligned cylinders with $m=4/3$, about the value for ice grains, with an assumed distribution of radii. Evidently, the general shape of the $P(\lambda)$ curve is very similar to that of $Q_{eE}-Q_{eH}$ in Fig. 8.1; the distribution of particle sizes broadens the theoretical curve and smoothes out the wiggles

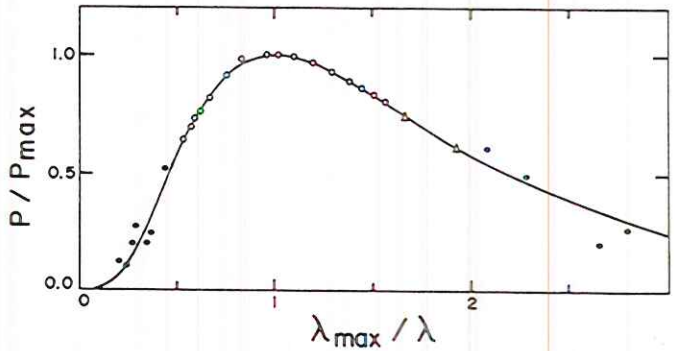

Figure 8.2 Normalized wavelength dependence of polarization. The ratio of polarization P observed in each star, to P_{max}, the maximum value in that star, is plotted against λ_{max}/λ, where λ_{max} is the wavelength at which P_{max} is observed. The open circles and triangles represent averages of 60 and 25 values, respectively, while the filled circles represent individual stars [5]. The solid curve gives a theoretical P/P_{max} for extinction by partially aligned cylinders with $m=1.33$.

which result from interference effects. Thus the maximum value of $Q_{eE}-Q_{eH}$ at $x\approx 2.5$ yields an effective mean cylinder radius of about 2×10^{-5} cm for $\lambda_{max}=5500$ Å. The fit shown in Fig. 8.2, although satisfactory, is not unique, and there is some question as to whether ice grains produce much of the observed selective extinction [S7.2b]. Particles of smaller a must be present to explain the ultraviolet observations, and the presence of some silicates is indicated by the 9.7-μ absorption as well as by theories of grain formation and development. A similar close fit can be obtained [6] with cylinders of about half the radius found above, but with m increased to 1.6, a typical value for silicates in the visible, giving about the same value of $(m-1)x$ at each wavelength.

The difference of λ_{max} between different stars suggests a corresponding difference in the sizes of the dust grains between different clouds. Corresponding small differences in the selective extinction curves observed for different clouds appear to be present. More specifically, stars in which λ_{max} exceeds the average value have relatively more extinction in the infrared. Thus for stars with $\lambda_{max}=7000$ Å, the mean $E(\lambda,V)/E_{B-V}$ decreases more steeply than normal as λ increases above 1μ, approaching about -4 with increasing λ, indicating an excess of larger radii among the visual grains. Evidently R_V, defined in equation (7-20), varies with λ_{max}; detailed measures give [7]

$$R_V=\frac{5.5\lambda_{max}(\text{Å})}{10{,}000\ \text{Å}}, \qquad (8\text{-}6)$$

yielding a variation in R_V from 2.5 to 3.9 as λ_{max} varies from 4500 to 7000 Å. A mean value of 5500 Å for λ_{max} corresponds to the usually adopted value of 3 for R_V; consideration of the further variation of $E(\lambda,V)$ out to 11.4μ would increase all these values of R_V slightly [S7.3a].

This correlation between selective extinction and the wavelength of maximum polarization cannot readily be explained by stellar peculiarities and appears to provide firm evidence for a difference in grain properties between different interstellar clouds.

Similar changes seem to be present between the outer and inner, presumably denser, regions of a single large cloud. In particular, within the extended obscuring cloud surrounding ρ Oph, systematic changes of λ_{max} and of the infrared extinction have been observed with increasing extinction [8]. Thus for moderately reddened stars, for which E_{B-V} is in the range 0.2 to 0.4 mag, and which are presumably near the boundary of this cloud, λ_{max} averages 6200 Å. For stars with E_{B-V} in the range from 1.0 to 1.3 mag, which are presumably behind denser inner regions of the cloud, λ_{max} rises to 8000 Å. The infrared extinction also changes with changing E_{B-V} and λ_{max} in a manner consistent with equation (8-6). These data may be interpreted as observational evidence for larger particle sizes in the denser regions of the cloud.

The observed change with wavelength of the direction of polarization also provides evidence for a change of grain properties with position. About 13 percent of the stars examined show smooth variations in the direction of the electric vector with wavelength over the spectral range from 3300 to 9800 Å, with a total angular change ranging between 3° and 27°, averaging about 10° [9]. While it is difficult to derive quantitative results about the interstellar medium from these data, it seems clear that regional variations are required both in the direction of alignment and in the wavelength dependence of ΔQ_e, the change in Q_e with changing inclination between B and the plane of vibration; ΔQ_e depends both on $Q_{eE}-Q_{eH}$ for individual dust grains and on the degree of alignment.

While the variation of λ_{max} from one region to another is well correlated with the shape of the normalized extinction curve from visual wavelengths into the infrared, the correlation with extinction in the far ultraviolet seems much weaker. We compare σ Sco (a star embedded in the ρ Oph cloud discussed above), whose normalized extinction curve in the far ultraviolet is about that of θ Ori (see Fig. 7.2), with ζ Oph, whose normalized extinction at 1100 Å is about 20 percent above the average. The values of λ_{max} for these two stars are 5600 Å for the former and 5900 Å for the latter [7]; this difference is relatively small and is in the opposite direction one might expect if the relative lack of far UV grains [S7.2b] in σ Sco were accompanied by a larger diameter for the visual grains. This result contrasts with that for θ Ori [S7.2b], where the absence of either the UV peak

grains or the far UV grains is apparently accompanied by an appreciably larger radius for the visual grains.

c. Dependence on Galactic Longitude

While λ_{max} apparently shows systematic variations over the sky [7], we shall consider here only the variation of the direction of polarization; that is, the orientation of the plane of vibration. As shown in Section 8.3a, the interstellar grains are likely to precess around the magnetic field **B** regardless of the specific process responsible for alignment. Hence the direction of polarization gives information on the direction of **B**. This general argument does not indicate whether **B** is parallel to the plane of vibration (which is mostly parallel to the galactic plane) or perpendicular to it. However, the Faraday rotation measures leaves little question but that **B** is parallel to the galactic plane; hence the plane of vibration must be parallel to **B**.

In order to average data from different stars, the Stokes parameters Q and U are introduced, defined by the relations

$$\frac{Q}{I} = P\cos 2\left(\theta_P - \frac{\pi}{2}\right), \tag{8-7}$$

$$\frac{U}{I} = P\sin 2\left(\theta_P - \frac{\pi}{2}\right), \tag{8-8}$$

where I is the total intensity, defined in equation (8-2), and θ_P is the angle between the plane of vibration projected on the plane of the sky and the great circle from the star to the north galactic pole. Evidently Q is positive if this plane of vibration is parallel to the galactic plane ($\theta_P = \pi/2$), and negative if perpendicular to this plane ($\theta_P = 0$). When the line of sight to a star passes through several clouds, each producing a polarization P_j with a position angle θ_{Pj}, it may be shown [10] that the resulting values of Q/I and U/I are simply the sums of Q_j/I and U_j/I over all clouds, provided the polarization is small, as is generally the case.

Mean values of the Stokes parameter q, in magnitudes ($q = 2.17\,Q/I$), are plotted in Fig. 8.3 as a function of galactic longitude l; each point represents an average for some 25 stars, all further away than 600 pc and with b less than 3° [11]. The double-sine-wave curve drawn in the figure corresponds to what would be expected if the grains were prolate spheroids, oriented with their major axes perpendicular to a magnetic field in the direction $b = 0°$, $l = 50°$; evidently the mean Q falls to a relatively low value between the maxima. For the closer stars the observed minima in Q are more nearly at about 60° and 240°. The direction of the local

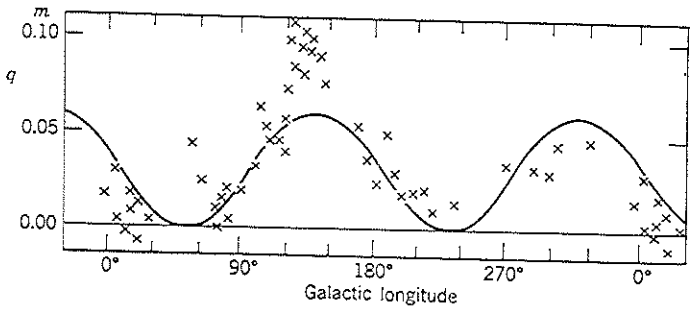

Figure 8.3 Dependence of polarization on galactic longitude [11]. Mean values of the Stokes parameter q (the difference in magnitudes of stellar intensity for **E** parallel and perpendicular to the galactic plane) are plotted for stars in different intervals of galactic longitude l. Each point represents an average for a group of about 25 stars, all at galactic latitudes less than 3° and at distances greater than 600 pc. The double sine wave is arbitrarily drawn with minima at $l = 50°$ and 230°.

Orion arm is roughly 70° [S1.5]. The magnetic field directions determined from these optical polarization data and from the Faraday rotation measurements in pulsars [S3.6a] are somewhat discordant, with a field indicated in the direction of l equal to 50° and 94°, respectively. While the observational uncertainty is appreciable, the magnetic field configuration is certainly more complicated than the simple uniform **B** assumed in analyzing the data.

The optical polarization observations give quantitative data on the nonuniformities in the magnetic field. The mean value of U/I is nearly zero for stars at low galactic latitude, as would be expected for a mean magnetic field parallel to the galactic plane. However, the rms dispersion of U/I, denoted by σ_U, is appreciable as a result of the different directions of **B** in different regions. The magnitude of σ_U may be used to determine the rms fluctuations of the position angle θ_{Pj} from one region to another, provided a number of statistical assumptions are made. An idealized model will be assumed in which the polarization is produced by a random distribution of clouds, each producing the same P_j, but with a distribution of θ_{Pj} about some mean value. We consider a group of stars in the galactic plane, all at the same distance, viewed in a direction perpendicular to **B**. If **B** is parallel to the galactic plane, the mean θ_{Pj} is $\pi/2$ radians, and we define

$$\alpha^2 = \left\langle \left(\theta_{Pj} - \frac{\pi}{2}\right)^2 \right\rangle, \tag{8-9}$$

where the brackets denote a mean value for all the stars considered.